Construction and Building Materials 38 (2013) 879–889

Contents lists available at SciVerse ScienceDirect

Construction and Building Materials

journal homepage: www.elsevier.com/locate/conbuildmat

Calculating crack extension resistance of concrete based on a new crack propagation criterion

Wei Dong [a,b,*], Zhimin Wu [a], Xiangming Zhou [b]

[a] State Key Laboratory of Coastal and Offshore Engineering, Dalian University of Technology, Dalian 116024, PR China
[b] School of Engineering and Design, Brunel University, London UB8 3PH, UK

HIGHLIGHTS

- The initial fracture toughness was proposed as crack propagation criterion for concrete.
- A FE analysis was carried out to simulate the complete fracture process in concrete.
- K_R-curve which is able to consider the variation of FPZ was investigated.
- The shape of K_R-curve was found to be affected by the FPZ variation and boundary effect.
- K_R-curve was found to be size dependent.

ARTICLE INFO

Article history:
Received 15 May 2012
Received in revised form 20 August 2012
Accepted 20 September 2012
Available online 30 October 2012

Keywords:
Concrete
Initial fracture toughness
Crack propagation criterion
K_R-curve
Fracture process zone (FPZ)
Crack extension resistance
Complete fracture process

ABSTRACT

A crack propagation criterion was proposed for model I crack in concrete by using the initial fracture toughness K_{IC}^{ini} as an inherent material property. Based on this criterion, crack begins to propagate when the difference, between the stress intensity factors caused by the applied load K_I^P and that by the cohesive stress K_I^σ, exceeds K_{IC}^{ini}. Finite element analyses was then carried out to calculate the complete load vs. crack mouth opening displacement (*P-CMOD*) curve, the critical crack propagation length Δa_C and the unstable fracture toughness K_{IC}^{un} for notched beams under three-point bending. It was found that numerical results showed a good agreement with the experimental ones. Based on this crack propagation criterion, crack extension resistance, in terms of stress intensity factor, K_R being able to consider the variation of fracture process zone (FPZ) was employed for describing crack propagation in concrete. K_R is composed of K_{IC}^{ini} and K_I^σ, which is actually equal to the driving action of crack extension. It was concluded that given the elastic modulus E, the uniaxial tensile strength f_t, the fracture energy G_F and K_{IC}^{ini}, the complete fracture process in concrete and the K_R-curve of concrete can be calculated based on the numerical method. Finally, discussion was made on the effects of fracture process zone, G_F and specimens geometries on K_R-curve.

1. Introduction

Crack extension resistance curve (*R*-curve) has been used as the fracture criterion for decades. This approach based on *R*-curve was first proposed by Irwin [1] to describe the crack propagation in metals under conditions of small-scale. Since then, it has been widely applied to quasi-brittle materials like concrete. The *R*-curve, in terms of either strain energy release rate *G* or stress intensity factor (SIF) *K*, has already been established as a basic fracture characteristics for a given specimen geometry. Bažant and Kazemi [2,3] and Bažant and Jirásek [4] derived geometry dependent *R*-curve based on the size effect law observed from fracture tests. The *R*-curve is then obtained as the envelope of the fracture equilibrium curves for geometrically similar specimens but with various sizes. On the other hand, Ouyang et al. [5] defined the *R*-curve as an envelope of energy release rates with different specimen sizes but the same initial notch length. Jenq and Shah [6] proposed the two-parameter fracture model (TPFM) in which the *R*-curve is derived by assuming that an effective traction-free critical crack is proportional to the initial crack length. Wecharatana and Shah [7] proposed a method to calculate *R*-curve which is able to consider the nonlinear effect of fracture process zone length. Jenq and Shah [8] predicted the *R*-curve using the constant K_{Ic} criterion, in which K_{Ic} was calculated based on the measured maximum load, the initial notch length using the formulas developed from linear elastic fracture mechanics (LEFM). Elices and Planas [9] and Planas et al. [10] analyzed the difference between cohesive materials and linear elastic ones using *R*-curve, and predicted the fracture behaviors of the cohesive

* Corresponding author at: State Key Laboratory of Coastal and Offshore Engineering, Dalian University of Technology, Dalian 116024, PR China.
E-mail addresses: dongwei@dlut.edu.cn, wei.dong@brunel.ac.uk (W. Dong).

0950-0618
http://dx.doi.org/10.1016/j.conbuildmat.2012.09.037

materials. Tvergaard and Hutchinson [11] utilized the highly refined finite element calculations and investigated the *R*-curve, for the crack growth in small-scale yielding under plane strain condition. Foote et al. [12] developed a theoretical model to calculate the *R*-curve using softening stress (σ)–crack opening displacement (w) relationship in strain-softening materials.

It should be noted that the conventional *R*-curve can only determine the onset of crack instability. In order to describe the increase of fracture toughness during crack propagation, a new approach was proposed by Xu and Reinhardt [13] and Reinhardt and Xu [14] to evaluate the crack extension resistance in terms of considering the cohesive stress acting on the fracture process zone (FPZ). In this method, K_R is obtained by combining the crack initiation fracture toughness K_{IC}^{ini}, which is an inherent material property, with K_I^{σ} which represents the contribution of the cohesive stress along the fictitious crack zone. A semi-analytical method was applied to calculate K_R-curve through using the curve of load vs. crack mouth opening displacement (*P-CMOD*) measured from experiment [13,14]. The result indicated that the K_R-curve is an inherent material property and size-independent. However, some scholars questioned whether the K_R-curve should be taken as an inherent material property. In the study of Mai [15], the SIF superposition method was applied to calculate K_R-curve by assuming FPZ to be a fictitious crack, and it was concluded that K_R-curve is not a material property, except for very large size specimens in which the crack-bridging zone is much smaller than the crack length and other dimensions. Furthermore, Hu and Wittmann [16] derived the extension of FPZ with the conventional compliance method in conjunction with a multi-cutting technique and proposed a new approach to calculate the K_R-curve by introducing a parameter to consider the residual deformation. The results suggested that the size dependency of K_R-curve is due to the difference in initial ligaments in concrete specimens. Following the studies of Xu and Reinhardt [13] and Reinhardt and Xu [14], Kumar and Barai [17,18] introduced the universal weight function to calculate the values of double-*K* fracture parameters. The weight function approach was also used to calculate the K_R-curve [19] based on cohesive stress distribution during crack propagation. The size effect was observed from specimen with different sizes, especially during the unstable fracture stage. Furthermore, the effects of geometry and loading condition on the K_R-curve in concrete were discussed by Kumar and Barai [20,21].

In the formula of K_R-curves proposed by Xu and Reinhardt [13] and Reinhardt and Xu [14], K_I^{σ} is a variable which is affected by FPZ length, and the relationship between fictitious crack opening displacement and stress acting on it, i.e., the cohesive law. Therefore, it is crucial to accurately determine FPZ and their associated cohesive laws for modeling the K_R-curves of concrete. Moreover, it is noticed that the K_R-curve is greatly affected by variation of FPZ length during crack propagation. Therefore, the difference in methods for determining FPZ length can affect the calculated results and shapes of K_R-curve. Xu and Reinhardt [13] and Reinhardt and Xu [14] studied the K_R-curve and FPZ length by means of fictitious crack model based on the assumption that the length of FPZ is constant when full FPZ is developed, i.e. the crack tip opening displacement (*CTOD*) exceeds the stress-free crack width w_0 in the softening traction-separation law. As a result, the K_R-curve rises monotonically with the increase of the ratio of the effective crack length to the beam depth, i.e. a/D. However, many experimental and theoretical studies have demonstrated that the FPZ length increases before FPZ is fully developed and decreases after that. For instance, Wecharatana and Shah [7] suggested that FPZ includes both the mechanical interlock zone and the zone where microcracking and other inelastic deformation occurred. The analysis in crack propagation of cement-based composites using their method showed that the FPZ length decreases with the increase of the crack length in the loading descending branch. A more accurate analytical technique was developed by Ballarini et al. [22] to predict crack growth in cement-based composites. They also came out the same conclusion on variation of FPZ length as Wecharatana and Shah [7]. They concluded that the crack length and the displacement were so large that the interlocking effect decreased within the FPZ. Hu and Wittmann [23,24] also presented a model to predict FPZ length. Their analytical and test results both indicated that the FPZ length increases before full FPZ develops but decreases after that. Using the method proposed by Xu and Reinhardt [13] and Reinhardt and Xu [14] but considering the variation of FPZ during crack propagation, Xu et al. [25] calculated the K_R-curve based on *P-CMOD* curve obtained from experiment. Their results also revealed that the K_R-curve is size independent. It should be noted that, in their study, Xu et al. [25] assumed fracture energy G_F as 100 N/m for concrete irrespective of mixtures rather than this value normally being derived from *P-CMOD* curve from notched beam test.

Moreover, due to sharp geometry, stress singularity may exist at the tip of crack in concrete or composite structures. For a concrete structure with cracks, crack propagation often occurs under service load. Therefore, the problem of stress singularity has been investigated in various studies [26,27], in which numerical methods are usually adopted. Several different numerical methods have been utilized to simulate crack propagation in concrete among which finite element method (FEM) is probably the most popular one. In traditional FEM, since fine meshes are needed to minimize the dependence of crack paths on initial mesh, re-meshing algorithm is necessary to accommodate crack propagation [28]. In general, re-meshing algorithm needs complex data structures to manage mesh updating as well as a well-validated crack propagation criterion. Fine crack tip meshes are also needed to represent the singularity in the stress filed, which may result in high computational cost. In order to overcome the drawbacks of re-meshing, an extended FEM [29] was developed to represent cracks by enriching the nodes in the discretization with discontinuous functions. Moreover, boundary element method (BEM) is a competitive alternative to FEM in simulating crack propagation. Combining the advantages of both FEM and BEM, a scaled boundary finite element method (SBFEM) was developed by Wolf and Song [30]. SBFEM has been successfully applied to simulate the dynamic crack propagation [31] and mixed-mode automatic crack propagation [32].

The main objective of this paper is to develop a numerical method to simulate the whole crack propagation in concrete by considering the variation of FPZ length. It was found that, using K_{IC}^{ini} derived from experiment as the parameter to determine crack propagation, the whole crack propagation can be simulated without the need of *P-CMOD* curve from experiment. On the other hand, notched concrete beams with depths D of 100, 200, and 300 mm, respectively, and initial crack ratios a_0/D of 0.2, 0.3, 0.4, and 0.6, respectively, were tested under three-point bending and *P-CMOD* curves were obtained which were then compared with the numerical ones to validate the proposed numerical method. After that, the proposed method was employed to obtain K_R-curve for the complete fracture process, which takes into account the cohesive stress acting on FPZ. Finally, the effect of variation of FPZ length and fracture energy on K_R-curve, as well as size effect of K_R-curve, was discussed.

2. New crack propagation criterion and experimental verification

2.1. Crack propagation criterion

In order to simulate fracture process, certain crack propagation criterion is needed which could be energy- or SIF-based. Based on

the principle of energy conservation, Xie derived the energy-based cohesive crack propagation criterion [33] which states that crack propagates when the strain energy release rate exceeds the energy dissipation rate in FPZ. The criterion has been successfully utilized to simulate crack propagation in concrete [34]. On the other hand, SIF-based crack propagation criterions are also widely adopted among which the crack tip stable criterion is very popular [35]. According to this criterion, when SIF caused by deriving forces exceeds the one by cohesive forces, i.e. $K_I \geqslant 0$, crack will propagate. It represents the competition between the crack driving forces which attempt to open the crack and the cohesive forces which attempt to close the crack. This criterion has been successfully used to simulate the crack propagation in reinforced concrete [36], mode-I and mixed-mode fracture [29,37,38] and multiple cohesive crack propagation [39] in concrete. It should be noted that the initial fracture toughness of concrete should be small enough so that it can be ignored when the criterion of $K_I \geqslant 0$ is adopted. However, in early stage of crack propagation, crack propagation length is short so that, comparing the SIF caused by cohesive force and applied load, the initial facture toughness may not be small enough to be ignored, especially for mode-I fracture in plain concrete. Moreover, the criterion of $K_I \geqslant 0$ can be used to determine crack propagation rather than crack initiation. Therefore, when using this criterion, crack is usually assumed to initiate when the maximum principal stress at the tip of crack exceeds uniaxial tensile strength of concrete [36–39].

Various experimental investigations have revealed that the fracture process in concrete structures included three different stages: crack initiation, stable crack propagation and unstable crack propagation or fracture. In order to differentiate the fracture process, the double-*K* fracture criterion was proposed which utilizes K_{IC}^{ini} and K_{IC}^{un} to describe fracture process of concrete [40,41]. Here, K_{IC}^{ini} is determined based on the initial cracking load, P_{ini}, and the initial cracking length a_0, while K_{IC}^{un} based on the measured maximum load, P_{max}, and the critical effective crack length a_C. However, it should be mentioned that a_C is difficult to be accurately measured from experiment. In order to circumvent this difficulty in measuring a_C, a linear asymptotic superposition method was introduced by Xu and Reinhardt [41] to take into account the nonlinearity of *P-CMOD* curve based on the following assumptions:

1. The nonlinear characteristic of the *P-CMOD* curve is caused by fictitious crack extension in front of a stress-free crack.
2. An effective crack consists of an equivalent elastic stress-free crack and equivalent elastic fictitious crack extension.

It is worth to mention that the linear asymptotic superposition method has been verified with both numerical and experimental results [17,18,40,41]. This method is therefore adopted in this study. Based on it, when load increases from zero to P_{ini}, i.e., from Point O to Point A (see Fig. 1), there is no crack propagation and LEFM can be used to calculate SIF at the tip of crack. At Point A, the crack length is a_0 and SIF K_{Ia}^{P} at crack tip caused by the applied load P can be obtained based on P_{ini} and a_0. At this point, the initial fracture toughness K_{Ia}^{ini} is equal to K_{Ia}^{P} when a is equal to a_0.

When P increases from P_{ini} to P_b, i.e., from Point A to Point B (see Fig. 1), crack will propagate and a fictitious crack length $\triangle a_b$ is reached. Therefore, according to the linear asymptotic method, the effective crack length now becomes a_b, which is equal to $a_0 + \triangle a_b$. If unloading takes place at this point, load will reduce linearly down to zero, i.e., from Point B to Point O as shown in Fig. 1. After that, if reloading, load will increase linearly to P_b, i.e., from Point O to Point B along Line OB as shown in Fig. 1. In other word, at Point B, the three-point bending beam can be regarded as a new virgin beam with an initial crack length a_b, but it should be noted

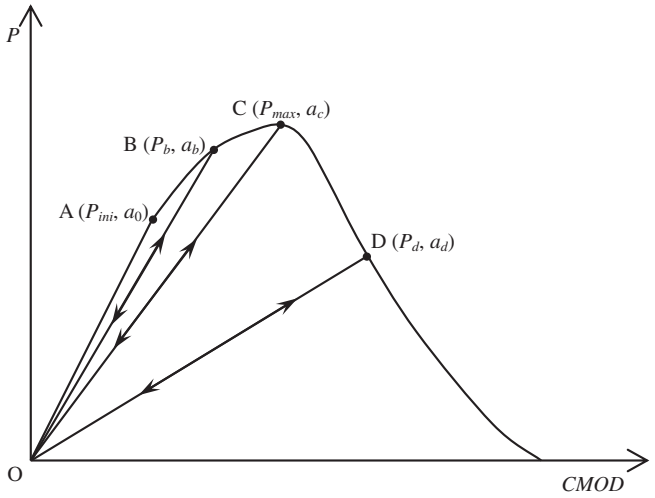

Fig. 1. Illustration of linear asymptotic superposition method.

that the internal cohesive stress acting on $\triangle a_b$ is exactly as an equivalent externally applied load, which presents the nonlinear fracture characteristics of concrete.

Therefore, at Point B,

$$K_{Ib}^{P} = K_{Ib}^{ini} + K_{Ib}^{\sigma} \tag{1}$$

Here, K_{Ib}^{P} is the SIF at the effective crack tip caused by load P_b, K_{Ib}^{ini} is initial fracture toughness when $a = a_b$, and K_{Ib}^{σ} is the SIF at the effective crack tip caused by cohesive stress acting on $\triangle a_b$.

At Point C, the peak point of *P-CMOD* curve, P reaches the maximum load, P_{max}, and the crack length a_c reaches the critical crack length a_C. The SIF at the effective crack tip caused by the applied load is equal to K_{IC}^{un}.

Therefore, at Point C,

$$K_{IC}^{un} = K_{Ic}^{P} = K_{Ic}^{ini} + K_{Ic}^{\sigma} \tag{2}$$

At Point D, which is at the descending branch of *P-CMOD* curve, SIF of K_{Id}^{P} caused by the applied load P_d is equal to K_{Id}^{σ}, caused by cohesive stress acting on $\triangle a_d$, plus the initial fracture toughness K_{Id}^{ini} when $a = a_d$, i.e.,

$$K_{Id}^{P} = K_{Id}^{ini} + K_{Id}^{\sigma} \tag{3}$$

Thus, based on the linear asymptotic superposition method, a complete fracture process of concrete, which is a nonlinear process, can be solved by LEFM. The *P-CMOD* curve of a three-point bending beam with initial crack length a_0, under monotonous loading, can be regarded as an envelope of *P-CMOD* curves for a series of geometrically similar three-point bending beams with various effective crack length. According to the double *K*-theory [40,41], initial fracture toughness K_{IC}^{ini} is an inherent material property irrespective of effective crack length. Therefore, the SIF at the effective crack tip of a three-point bending notched beam can be obtained using the following simple relationship based on linear superposition principle:

$$K_{I}^{P} = K_{IC}^{ini} + K_{I}^{\sigma} \tag{4}$$

If load P and the corresponding crack length a are known, the crack opening displacement can be calculated using FEM, and the cohesive stress distribution can be obtained by using the cohesive stress–crack opening relationship, σ–w. Then stress intensity factor K_I^{σ} caused by cohesive stress can be obtained, and K_I^{P} caused by the applied load P can be directly calculated by the quarter point singular element approach. Therefore, considering the whole crack propagation process as the accumulation of many new

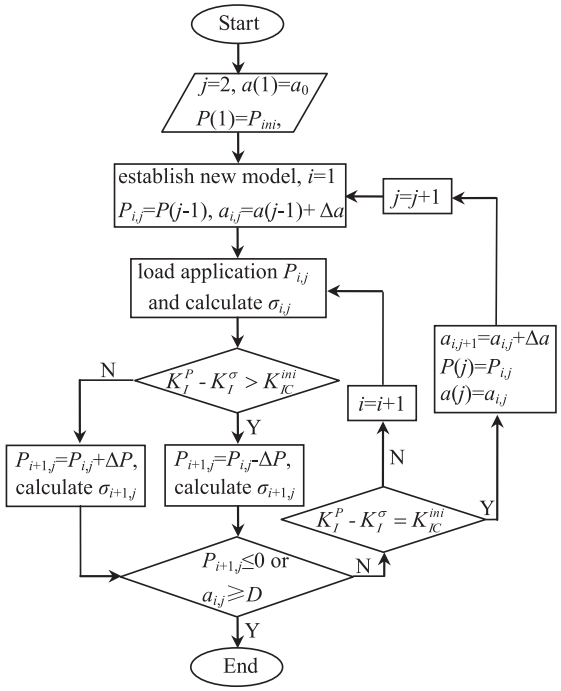

Fig. 2. Program flow diagram for the iterative process in the numerical method.

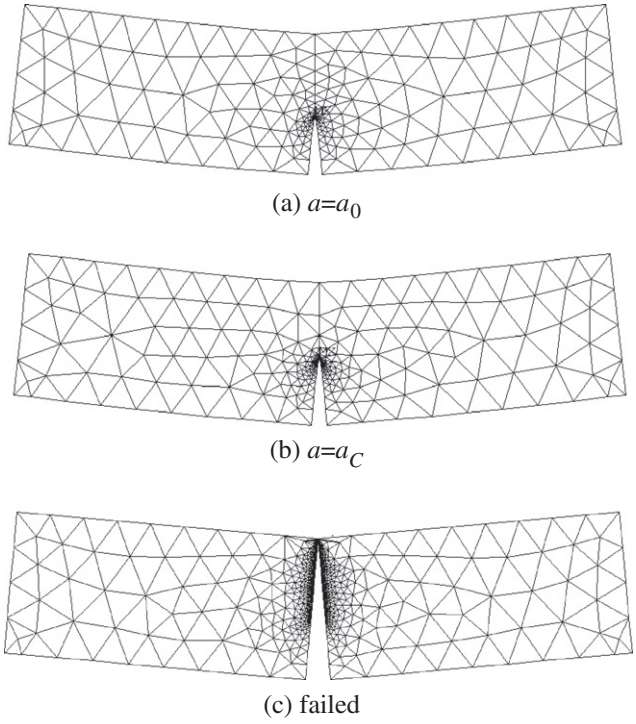

Fig. 3. Different stages in fracture process from numerical analyse.

micro-cracking initiations, for each crack length increment Δa, load will reach the critical value which makes crack propagate. Each crack propagation process includes crack initiation and crack propagation. K_{IC}^{ini} is the index for estimating crack initiation which is the crack propagation criterion proposed in this paper. Generally, the crack propagation criterion can be described as follows:

$$K_I^P - K_I^\sigma < K_{IC}^{ini}, \quad \text{crack does not propagate} \tag{5}$$

$$K_I^P - K_I^\sigma = K_{IC}^{ini}, \quad \text{crack is in the critical state} \tag{6}$$

$$K_I^P - K_I^\sigma > K_{IC}^{ini}, \quad \text{crack propagates} \tag{7}$$

The above crack propagation criterion is adopted to simulate the whole fracture process in the proposed numerical method reported in this study using an iterative process which is illustrated by the program flow diagram shown in Fig. 2. The following steps are included in the iterative numerical process:

1. Calculate K_{IC}^{ini} based on a_0 and P_{ini}, denoted as $P(1) = P_{ini}$, from experiment.
2. Establish FEM model for three-point bending beam with crack length $a_{i,j} = a(j-1) + \Delta a$ ($i = 1,2\ldots$, $j = 2,3,\ldots$). Here Δa is a

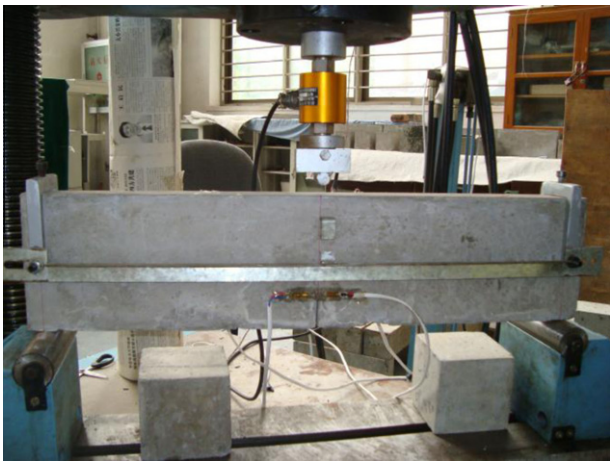

Fig. 4. Set-up of the three-point bending beam test.

Table 1
Sizes, material parameters and calculated a_{w0}/D for B-series beams.

Specimen	$L \times D \times B$ (mm)	a_0/D	K_{IC}^{ini} (MPa m$^{1/2}$)	G_F (N/m)	P_{max} (kN)	a_{w0}/D
B2-1	600 × 150 × 40	0.2	0.60	96	2.54	
B2-2			0.59	100	2.48	
B2-3			0.62	92	2.61	
Avg.			0.60	96	2.54	0.77
B3-1	600 × 150 × 40	0.3	0.65	100	2.39	
B3-2			0.63	105	2.04	
B3-3			0.53	88	1.89	
Avg.			0.60	98	2.11	0.82
B4-1	600 × 150 × 40	0.4	0.58	85	1.29	
B4-2			0.61	100	1.51	
Avg.			0.60	92.5	1.40	0.85
B6-1	600 × 150 × 40	0.6	0.60	105	0.77	
B6-2			0.62	120	0.89	
B6-3			0.58	100	0.77	
Avg.			0.60	108	0.81	0.92

Table 2
Sizes, material parameters and calculated a_{w0}/D for L-series specimens.

Specimen	$L \times D \times B$ (mm)	a_0/D	G_F (N/m)	K_{IC}^{ini} (MPa m$^{1/2}$)	P_{max} (kN)	a_{w0}/D
L1-1	400 × 100 × 100	0.4	104	0.52	2.73	
L1-2			90	0.52	2.81	
Avg.			97	0.52	2.77	0.87
L2-1	800 × 200 × 100	0.4	155	0.71	5.15	
L2-2			151	0.62	5.27	
Avg.			153	0.67	5.21	0.85
L3-1	1200 × 300 × 100	0.4	123	0.78	7.31	
L3-2			146	0.75	7.72	
L3-3			153	0.75	6.46	
Avg.			141	0.76	7.16	0.81

specified increment of crack length. i represents the load increment step during the iteration analyses in which the crack length keeps no change. j represents the crack length increment step during the iteration analyses.

3. Apply load $P_{i,j}$ to the notched beam and calculate cohesive stress $\sigma_{i,j}$. Calculate K_I^P and K_I^σ by adjusting load $P_{i,j}$ until the Eq. (6) is satisfied. When $K_I^P - K_I^\sigma < K_{IC}^{ini}$, load should be increased with a load incensement ΔP and cohesive stress $\sigma_{i,j}$ should be recalculated based on the displacement caused by $P_{i,j} + \Delta P$. When $K_I^P - K_I^\sigma > K_{IC}^{ini}$, load should be decreased with a load incensement ΔP and cohesive stress $\sigma_{i,j}$ should be recalculated based on the displacement caused by $P_{i,j} - \Delta P$. Once $K_I^P - K_I^\sigma = K_{IC}^{ini}$, the adjustment of the applied load will terminate and the adjusted load at the final step will be the actual load.
4. Repeat steps 2–3 for the next crack propagation. The iterative process terminates when the crack tip is closed to the boundary of beam or the value of the corresponding applied load becomes a negative value.

It can be seen from Fig. 2 that the applied load $P(j)$ and the corresponding crack propagation length $a(j)$ can be obtained in the (j)th steps. In the same step, the fracture parameters, such as $K_I^P(j)$, $K_I^\sigma(j)$ and $CMOD(j)$, are also obtained. The numerical method with the iterative process was applied to analyze the B-, L-, H-, and P-series notched beams under three-point bending and their whole fracture processes were obtained. A typical example from numerical analyses is shown in Fig. 3 which illustrates the evolution of the fracture process of the L3-series specimen (see in Table 2).

2.2. Experimental verification

In order to validate of the proposed method, two series of concrete beams, with different a_0/D (denoted as B-series) and sizes (denoted as L-series), where D is the depth of the notched beam, were tested under three-point bending and the corresponding *P-CMOD* curves were obtained. The set-up of three-point bending notched beam test is schematically illustrated in Fig. 4. On the other hand, *P-CMOD* curves were also obtained using the proposed numerical method in this study, through finite element analysis, with the crack propagation criterion mathematically described by Eqs. (5)–(7). The bilinear constitutive law for σ–w, proposed by Peterson [42], was utilized to determine the cohesive stress acting on FPZ.

In this study, singular element was used to calculate SIF at the tip of crack. Because high stress gradients exist in the region around crack tip, special attention should be paid in that region. Therefore, a circle was set at the tip of crack, in which the crack tip point is the center of the circle and the crack propagation length Δa is the radius of the circle. The first row of elements around the crack tip had a radius of $\Delta a/6$, and the mid-side nodes were placed

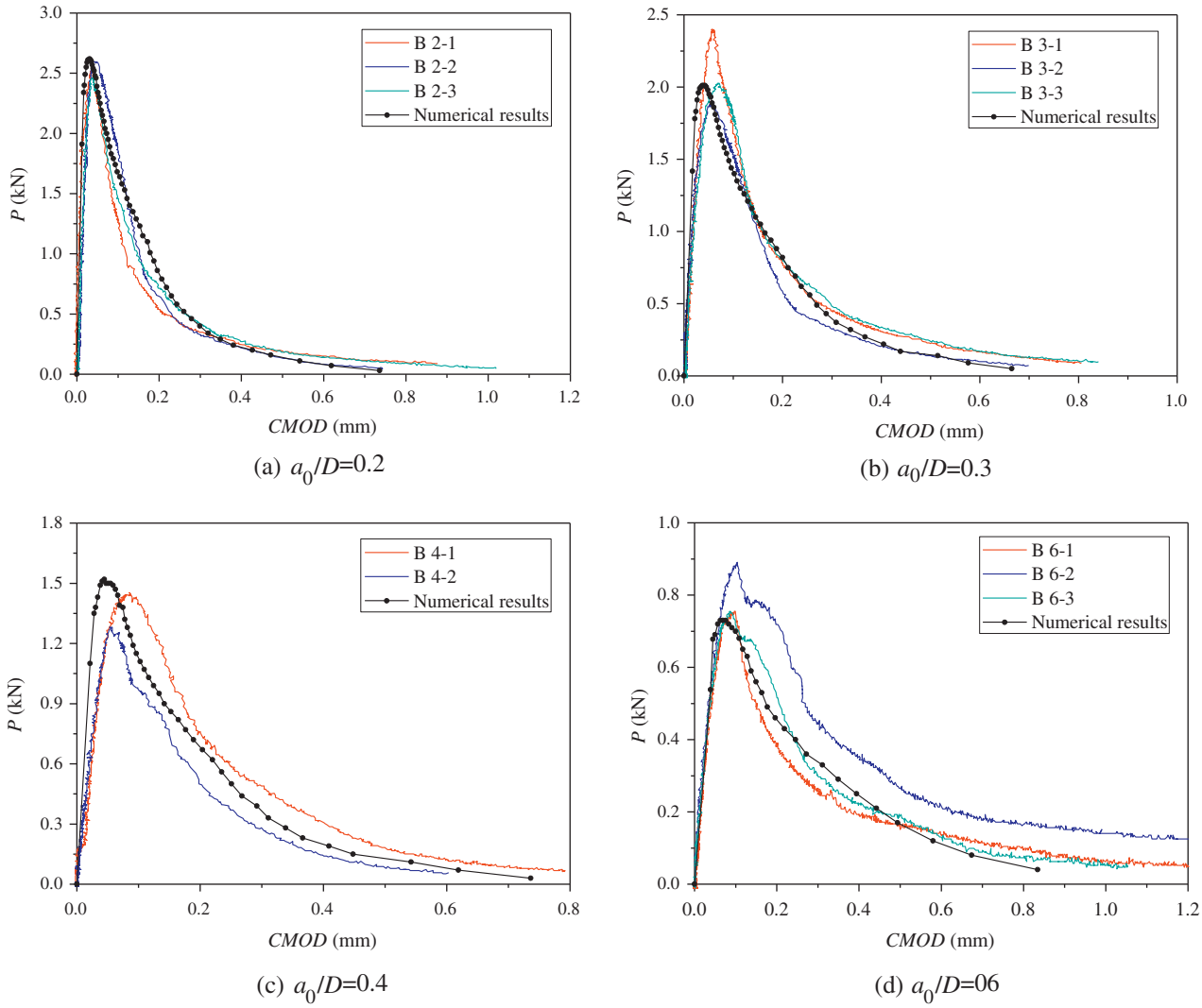

Fig. 5. *P-CMOD* curves for B-series beams.

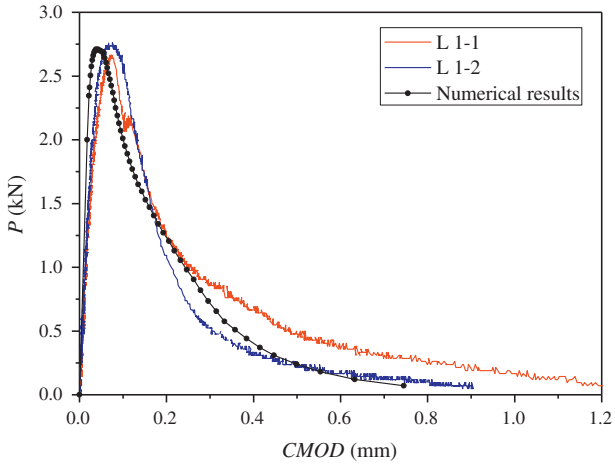

(a) D=100mm

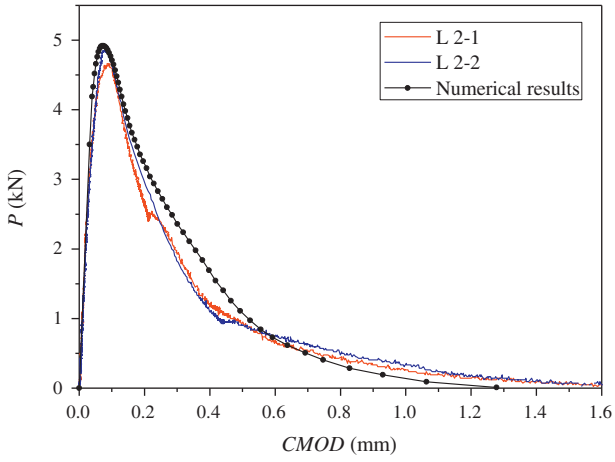

(b) D=200mm

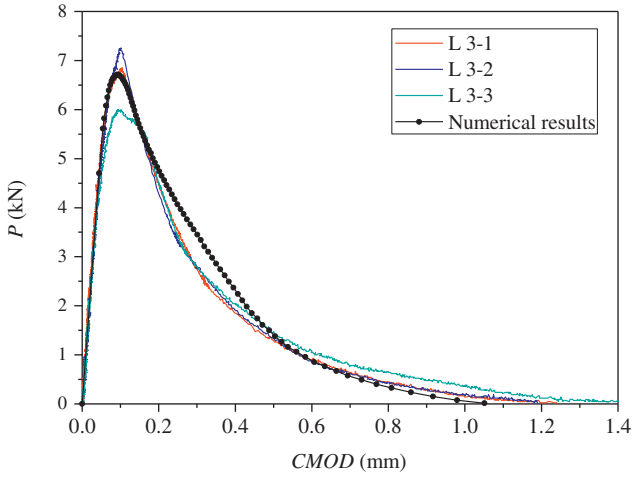

(c) D=300mm

Fig. 6. *P-CMOD* curves for L-series beams.

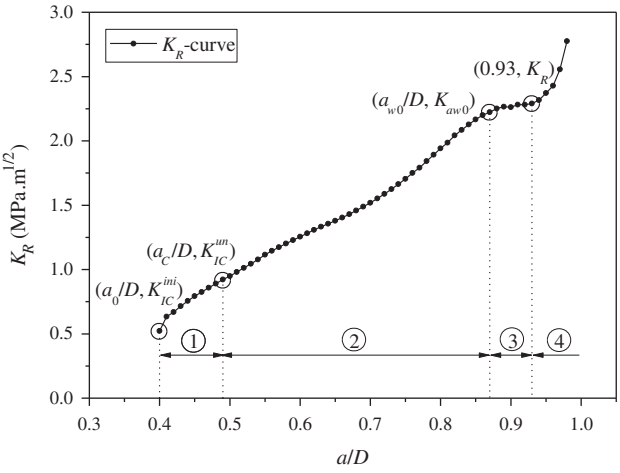

(a) D=100mm

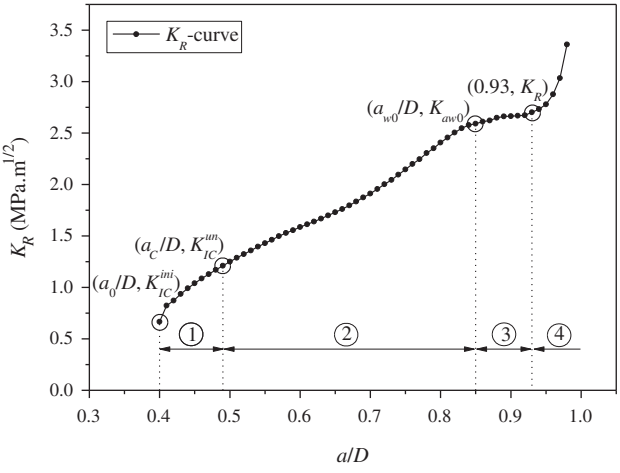

(b) D=200mm

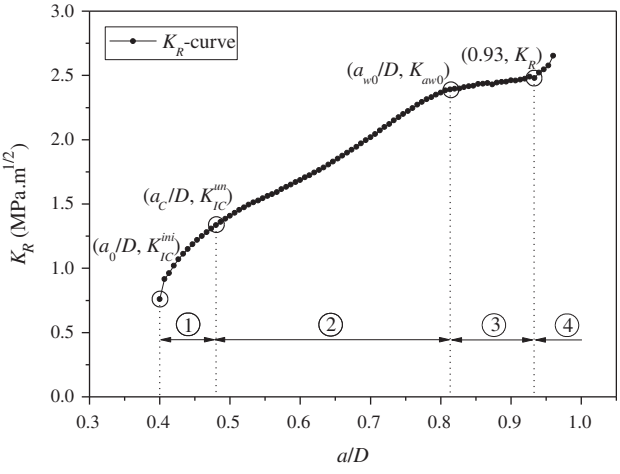

(c) D=300mm

Fig. 7. *KR*-curves for L-series beams.

at the quarter points, i.e. had a radius of $\Delta a/24$. In order to solve SIF at crack tip accurately, a crack propagation length Δa of (1–2%) D was used in this study.

For B-series specimens, the span L, depth D and width B were kept constant as 600 mm, 150 mm and 40 mm, respectively, but initial crack ratio a_0/D varied from 0.2 to 0.6 (see Table 1). The concrete was made of aggregate with the maximal size of 8 mm and had the mechanical properties of the uniaxial tensile strength f_t = 2.4 MPa, elastic modulus E = 28GPa, and Poisson's ratio v = 0.2. For L-series specimens, span-to-depth ratio L/D and initial crack ratio a_0/D were kept constant as 4.0 and 0.4, respectively, but the

depth D varied from 100 mm to 300 (see Table 2). The concrete was made of aggregate with the maximal size of 10 mm and had the mechanical properties as f_t = 2.3 MPa, E = 24GPa, and v = 0.2. In order to measure the initial load, four stain gauges were attached vertically in front of the precast notch on the both sides of specimen, and the distance of two strain gauges was 10 mm. When crack initiates and stars to propagate, the measured value of the strain gauge will decrease suddenly due to the fracture energy release. Therefore, the initial cracking load can be obtained according to the variation of the strain at the tip of precast notch. Initial fracture toughness can be calculated based on the initial crack length and initial load [40]. Table 1 shows the average results of different series.

The derived fracture parameters from experiments are presented in Tables 1 and 2. The complete *P-CMOD* curves obtained from both experiment and numerical simulation are presented in Figs. 5 and 6. In Tables 1 and 2, a_{w0} is the crack length corresponding to the cohesive stress when the initial crack tip decreases to zero. It can be seen that the *P-CMOD* curves obtained from numerical simulation agree well with those from experiment suggesting that the proposed numerical method, together with the crack propagation criterion, in this paper can be used for simulating the complete fracture process in concrete.

3. Crack extension curve of concrete

As aforementioned, the crack extension resistance can be expressed in terms of either strain energy release rate G or stress intensity factor K. Irwin [1] proposed an energy-based R-curve which is formulated as the following equation:

$$G = \Gamma_R(\Delta a) \tag{8}$$

where Γ_R is the crack growth resistance, i.e. total work of fracture per unit area of crack propagation. Later on, the crack extension resistance in terms of stress intensity factor, which has been widely applied in practice, was introduced which is stated in Eq. (9).

$$K_R = K_I^P(P, \Delta a) \tag{9}$$

G can be calculated from $G = K^2/E'$ according to the elastic fracture mechanics. Under plane strain and plane stress conditions, E' is equal to $E/(1-v^2)$ and E, respectively. Here, E is the elastic modulus and v is the Poisson's ratio.

Resistance curve, i.e., R-curve, can be presented if the stress intensity factors caused by P and Δa are obtained during the crack propagation process.

About the definition of K_R-curve, Xu and Reinhardt [13] and Reinhardt and Xu [14] claimed that Eq. (9) gave the stress intensity factors for different Δa, but not K_R-curve considering crack propagation in concrete, because material parameters relevant to concrete properties were not included in this equation. Therefore, a new K_R-curve was proposed by them [13,14] in which the K_R-curve was determined by combining the crack initiation toughness K_{IC}^{ini} which is an inherent material property of concrete, with the contribution due to the cohesive stress K_I^σ determined by f_t and a along the fictitious crack zone during the fracture process. The K_R is formulated as follows:

$$K_R(\Delta a) = K_{IC}^{ini} + K_I^\sigma \tag{10}$$

The crack propagation criterion is written as follows:

$$K_I^P(P, \Delta a) - K_I^\sigma = K_{IC}^{ini} \tag{11}$$

Therefore, from Eqs. (10) and (11), the following can be derived:

$$K_I^P(P, \Delta a) = K_R(\Delta a) \tag{12}$$

According to the crack propagation criterion, the applied load is the driving action that makes crack propagate by overcoming the resistance, i.e. the stress intensity factor caused by driving force is equal to the crack extension resistance. From Eq. (12), K_R-curve can be obtained once the load and the related crack length are determined. Therefore, determining the load for different crack propagation length is a key issue, in order to obtain K_R-curve, which can be achieved by using the proposed numerical method in this study combined with the proposed crack propagation criterion. For instance, the complete K_R-curves of L-series specimens obtained through numerical analyses are presented in Fig. 7a–c, and the variation of FPZ with respect to specimen height is shown in Fig. 8.

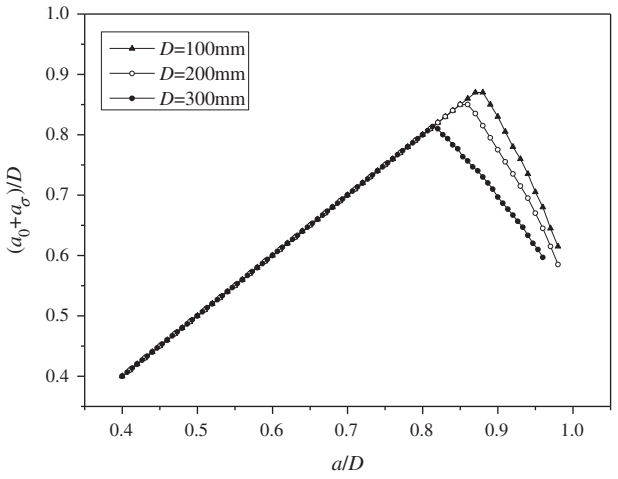

Fig. 8. Variation of fracture process zone for L-series beams.

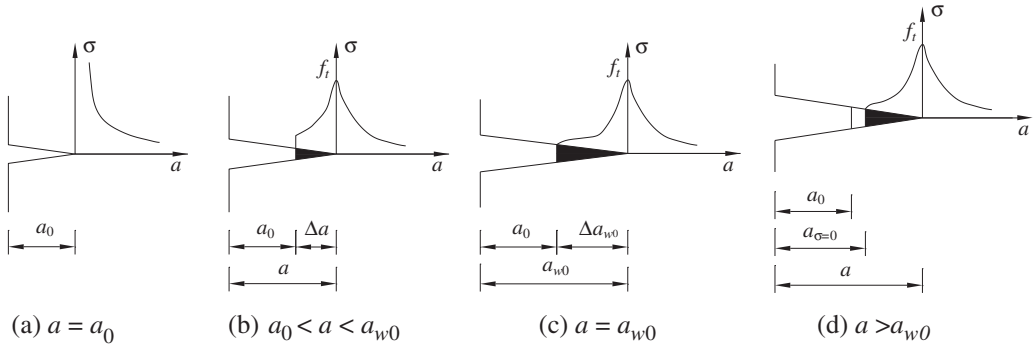

Fig. 9. Variation of fracture process zone in the fracture process.

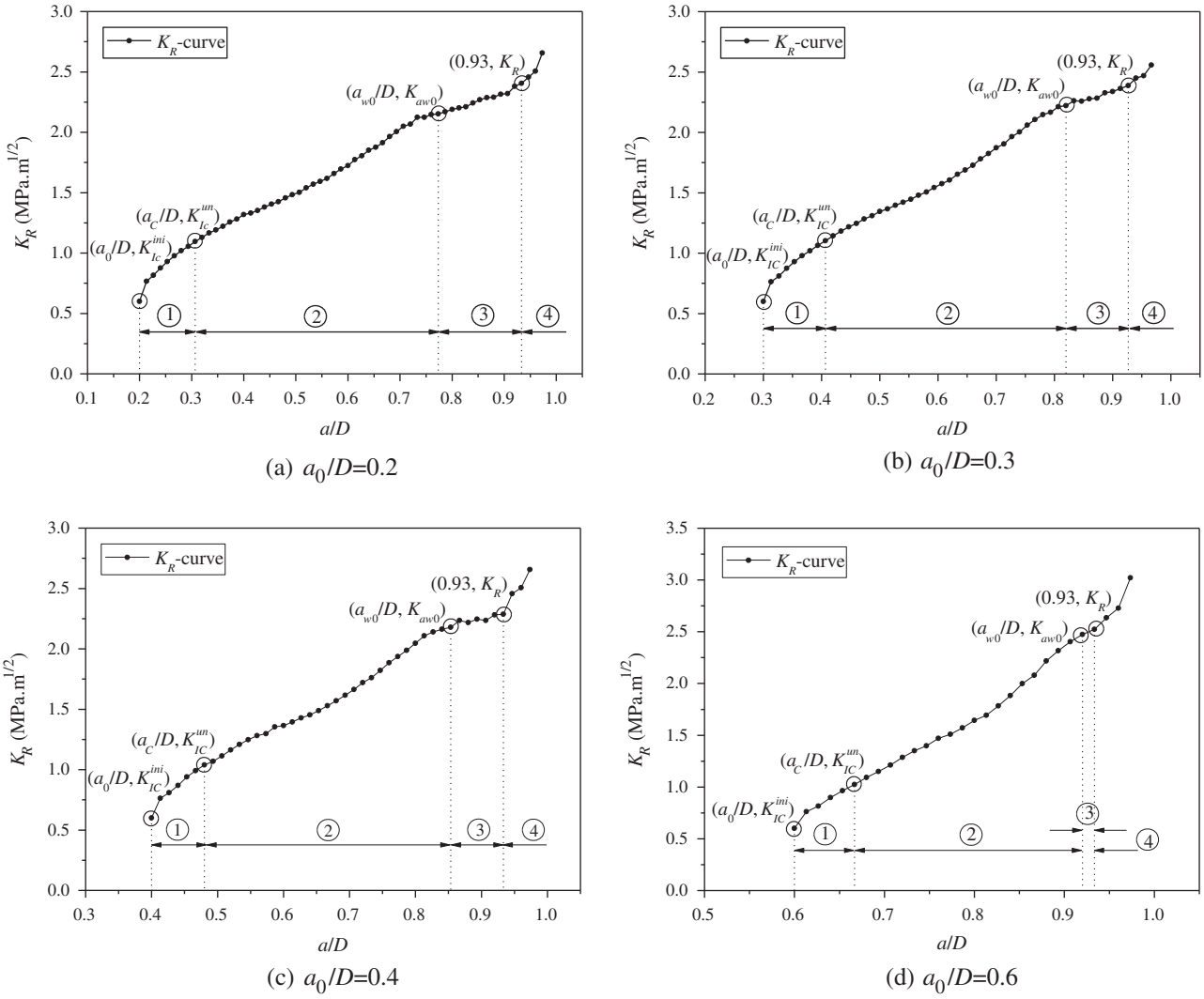

Fig. 10. *KR*-curves for B-series beams.

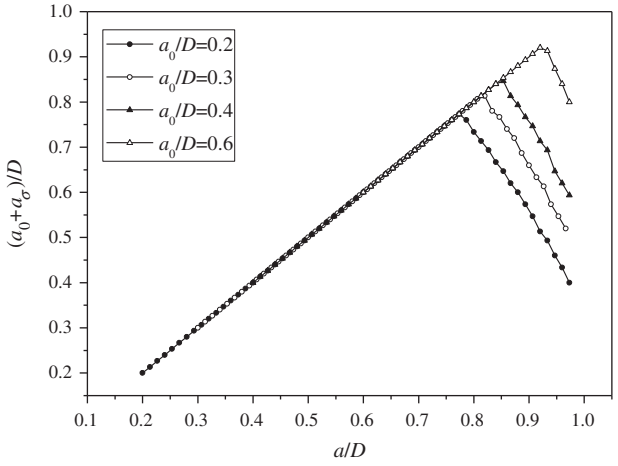

Fig. 11. Variation of fracture process zone for B-series beams.

Here, a_σ is the crack length acting on the cohesive stress, i.e. FPZ length.

Table 3
Sizes and calculated P_{ini}, P_{max}, and a_{w0}/D for H-series beams.

Specimen	$L \times D \times B$ (mm)	a_{w0}/D	P_{ini} (kN)	P_{max} (kN)
H200	800 × 200 × 200	0.72	10.00	15.12
H300	1200 × 300 × 200	0.67	12.20	20.11
H500	2000 × 500 × 200	0.61	15.80	27.87
H700	2800 × 700 × 200	0.57	18.70	34.19
H900	3600 × 900 × 200	0.54	21.20	39.82
H1000	4000 × 1000 × 200	0.53	22.30	40.61
H1200	4800 × 1200 × 200	0.50	24.50	45.18
H1500	6000 × 1500 × 200	0.47	27.30	51.51

4. The features of K_R-curve

4.1. Effects of FPZ on K_R-curve

Due to the effect of cohesive stress on fictitious crack zone, the crack extension resistance in concrete increases with the increase of the fictitious crack zone during crack propagation process. To evaluate the effects of FPZ on K_R-curve, the complete fracture process in concrete are divided into four stages as shown in Fig. 7.

At the first stage, a is between a_0 and critical crack length a_C. Before the applied load reaches P_{ini}, there is no crack extension. The

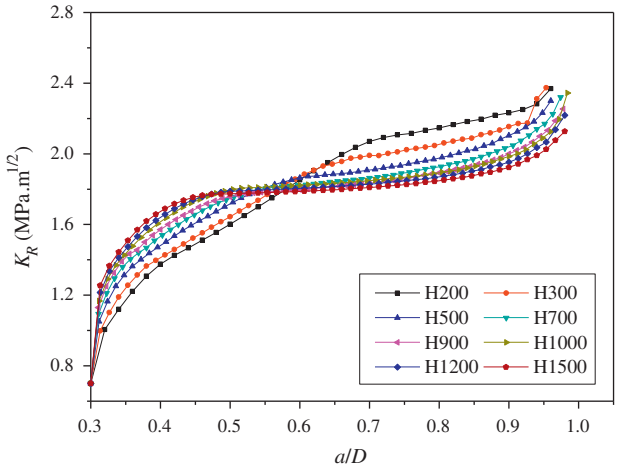

(a) K_R-curves

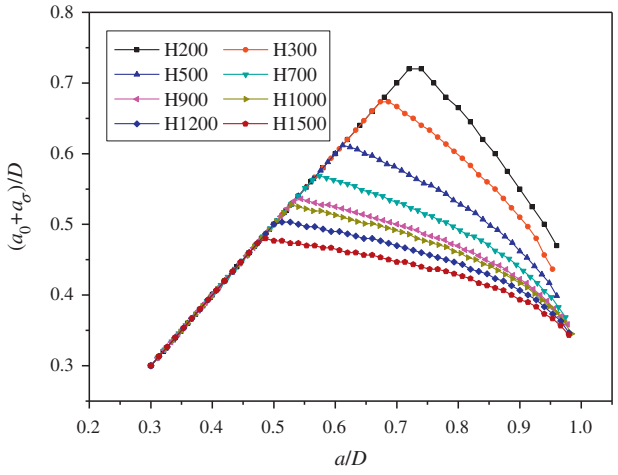

(b) Variation of fracture process zone

Fig. 12. Numerical results for H-series beams.

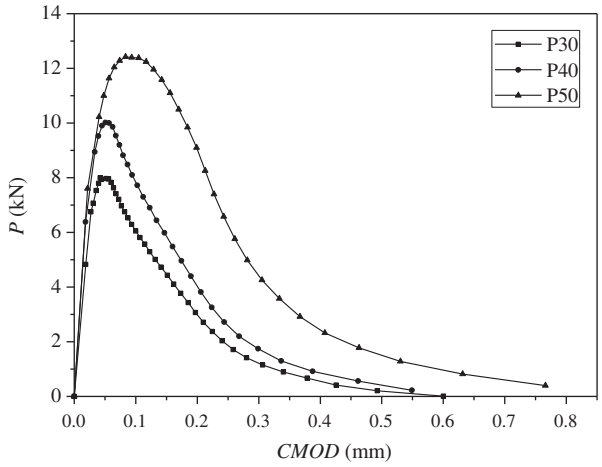

(a) *P-CMOD* curves

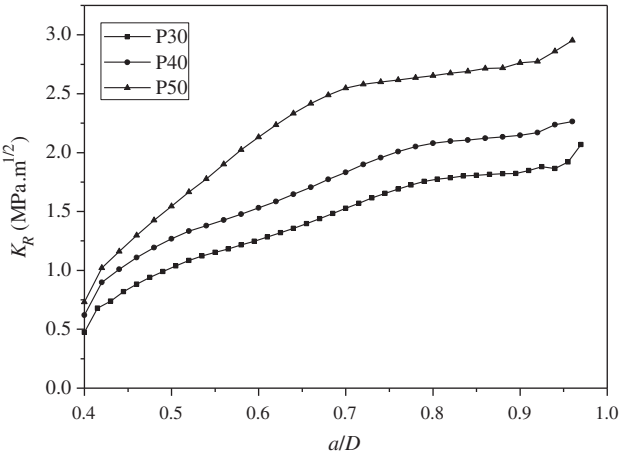

(b) K_R-curves

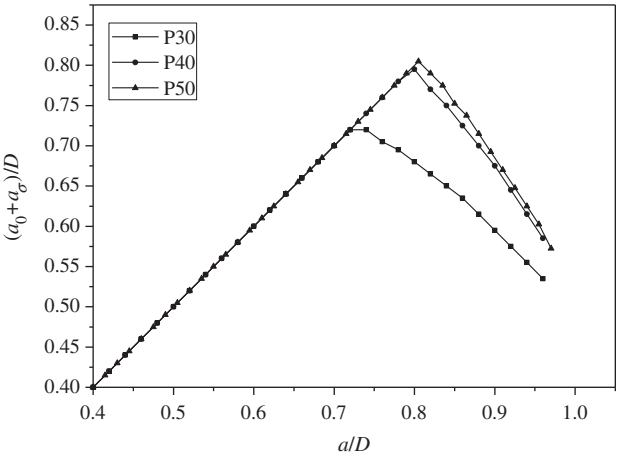

(c) Variation of fracture process zone

Fig. 13. The numerical results for P-series specimens.

FPZ length is equal to zero and K_R is equal to the initial toughness. After that, a stable crack extension is first reached and the FPZ length will increase with the crack propagation. Thus, the effective crack length is equal to the sum of the initial crack length and the effective crack extension, while the crack extension resistance increases due to the increase of the FPZ length. When the applied load reaches P_{max}, K_R is equal to K_{IC}^{un}, and unstable crack propagation is thus initiated.

At the second stage, a is between a_C and a_{w0}, the *CTOD* continues to increase up to the crack opening w_0 at zero stress, the effective crack length reaches a_{w0} and the cohesive stress at the initial crack tip decreases to zero. In this case, the FPZ is fully developed and its length reaches the maximum value. For L-series specimens (see Table 2), when the FPZ is fully developed, a_{w0}/D is equal to 0.87, 0.85 and 0.81, respectively, for L1-, L2-, and L3-series specimens. At this stage, as the crack propagates, the K_R-curve ascends sharply.

Table 4
Material parameters and numerical results of P_{max} and a_{w0}/D for P-series beams.

Specimen	$L \times D \times B$ (mm)	a_0 (mm)	E (GPa)	f_{cu} (MPa)	G_F (N/m)	a_{w0}/D	K_{IC}^{ini} (MPa m$^{1/2}$)	P_{ini} (kN)	P_{max} (kN)	
									Exp.	Num.
P30	800 × 200 × 200	80	29.6	30.9	71.4	0.844	0.47	4.83	7.65	7.99
P40			32.6	45.4	88.1	0.838	0.60	6.38	9.76	10.02
P50			34.3	52.6	95.9	0.809	0.69	7.60	11.07	12.42

At the third stage, $a_{w0} < a_0 < 0.93D$, when the *CTOD* exceeds a_{w0}, a cohesive stress-free zone is formed in front of the initial crack tip. In this case, the effective crack consists of the initial crack, newly formed stress-free crack and FPZ. The variation of fracture process zone for L-series beams are shown in Fig. 8. Here, the sum of a_0 and newly formed stress-free crack length is denoted as $a_{\sigma=0}$. Then, the variation of FPZ, after full FPZ is developed, becomes a key factor that affects K_R value. Compared with the second stage, the rising tendency of K_R-curve is not significant.

After that, there is a noteworthy phenomenon that the K_R-curves for specimens with different sizes exhibit rapid rising when $a/D > 0.93$. Therefore, at this fourth stage, i.e., when $a/D > 0.93$, the boundary effect is very significant, which is related to a/D rather than the ligament length. In the tests conducted in this research, the a/D corresponding to the initiation of boundary effect is 0.93. It can be seen from the results shown in Fig. 7 that the plateau is longer for specimens with greater size. In summary, for three-point bending beams in this test, the shape of K_R-curve is affected by the FPZ variation when $a < 0.93D$ but greatly by boundary effect when $a > 0.93D$. The FPZ variation during crack propagation is shown in Fig. 9.

The K_R-curves for B-series specimens are presented in Fig. 10. The variation of fracture process zone for B-series beams are shown in Fig. 11. It can be seen that the plateau is not significant owing to shorter ligament length. The a_{w0}/D is 0.77, 0.82, 0.85 and 0.92 when a_0/D is 0.2, 0.3, 0.4 and 0.6, respectively. Therefore, the third stage is shorter for greater a_0/D. When $a_0/D = 0.6$, a_{w0}/D is so closed to 0.93 that the plateau in K_R-curve disappears. For this case, the K_R-curve demonstrates continuous rise without a plateau.

4.2. Effect of the geometry on K_R-curve

The size effects on K_R-curve have been discussed by many researchers [6–8]. Although *R*-curve is defined differently by different researchers, it has been generally accepted that *R*-curve are both size-dependent and geometry-dependent. However, Xu and Reinhardt [13] concluded that K_R-curve is independent on specimen size or the initial crack ratio, i.e., a_0/D, based on the assumption that the FPZ length keeps constant after FPZ is fully developed. After that, using the same method but considering a varying full FPZ length, Xu et al. [25] investigated the K_R-curve and got the same conclusion as Xu and Reinhardt [13]. On the other hand, Kumar and Barai [19] derived K_R-curve using weight function method and found that the size effect on K_R-curve is more prominent during the crack unstable propagation stage. Therefore, further study is necessary on the size effect on K_R-curve due to inconsistent findings reported. The FPZ length may need to be considered as varied after it is fully developed.

In order to investigate the size effect on K_R-curve, H-series three-point bending beams with initial crack ratio $a_0/D = 0.3$ and the section depth varied from 200 mm to 1500 mm were analyzed by finite element analysis in which the following material parameters were adopted for concrete, $f_t = 3.25$ MPa, $G_F = 100$ N/m, $K_{IC}^{ini} = 0.7$, and $E = 30.5$GPa. The a_{w0}/D obtained through numerical analyses are listed in Table 3.

It can be seen from Fig 12a that the K_R-curves for specimens with different heights demonstrates different tendency, and curves meet approximately when a/D is about 0.57. The value of K_R for smaller beams is less than those for larger beams, when a/D is less than 0.57; but it become greater for larger size beams, when a/D is greater than 0.57 which can be explained by the difference in the FPZ distribution during crack propagation in beams with different depths as shown in Fig 12b. With the same a/D, the FPZ length in smaller beams is less than that in larger ones, and K_R is thus reasonably lower because of the shorter integration range at this early fracture stage when the developed FPZ length is short. With the decreasing of the beam depth, the value of a_{w0}/D increases. Therefore, the FPZ length is larger in beams with smaller size and K_R is greater because of longer integration range at this late fracture stage when the developed FPZ is long. Moreover, the full FPZ is developed for most specimens when a/D are between 0.5 and 0.6. It may be the reason why the K_R-curves meet at a point, where a/D is about 0.57.

4.3. Effects of the G_F on K_R-curve

The material parameters of P-series beams under three-point bending derived from experiment are listed in Table 4, among which G_F of the beams are 71.4 N/m, 88.1 N/m and 95.9 N/m, respectively. Fig. 13 shows various K_R, *P-CMOD* and FPZ curves obtained from numerical analyses for the P-series beams. With the increase of G_F, the cohesive effect along FPZ is intensified. Therefore, the K_R-curve clearly demonstrates the rising tendency (see Fig. 13b) and the value of a_{w0}/D decreases (see Table 4) correspondingly.

5. Conclusions

In this study, the initial fracture toughness K_{IC}^{ini} was adopted as the fracture propagation criterion for simulating crack propagation process in concrete. Based on this criterion, a new numerical method for calculating K_R-curve, which consists of the contributions of cohesive stress along the FPZ and initiation toughness of concrete, was proposed. Subsequently, the FPZ variation was examined and its effect on K_R-curve is investigated for the complete fracture process. Finally, the influence of several key fracture parameters on the K_R-curve was discussed. The following conclusions can be drawn:

(a) Given the elastic modulus E, the uniaxial tensile strength f_t, the energy release rate G_F and the initial fracture toughness K_{IC}^{ini}, the complete crack propagation process and the crack extension resistance K_R-curve of concrete can be simulated accurately using the proposed numerical method.
(b) Based on the crack propagation criterion, applied load overcomes resistance and makes crack extend during each micro-crack propagation step, i.e., the $K_R - \Delta a$ curve is actually equated to the stress intensity factor caused by the applied load P plots related to Δa.
(c) The shape of K_R-curve is affected by both the variation of FPZ and specimen boundary. The rising of K_R-curve is significant before the FPZ reaches its full length. After that, the K_R-curve will achieve a plateau with the FPZ shrinks. Ultimately, when a/D rises to around 0.93 for the beams in this research, the K_R-curve exhibits a rapid rise due to boundary effect.
(d) The K_R-curve tends to be different for three-point bending beams with depth from 200 mm to 1500 mm, which depends on the fracture ligament length of specimen. The K_R-curves meet at a point when a/D is around 0.57, and at that time the full FPZ has developed in most specimens. The value of K_R for smaller size beams is less than that for larger size beams when a/D is less than 0.57, but it becomes greater for larger size beams when a/D is greater than 0.57.

Acknowledgements

The financial support of the New Teacher Fund for Doctor Program from the Ministry of Education of China under the Grant 20110041120012, the National Natural Science Foundation of China under the Grant NSFC51109026, and the Engineering and

Physical Sciences Research Council UK under the Grant of EP/I031952/1 is great acknowledged.

References

[1] Reports of Special ASTM Committee on fracture testing of high-strength metallic materials: fracture testing of high-strength sheet materials. ASTM Bulletin No. 243, January, 1960. p. 29–40.
[2] Bažant ZP, Kazemi MT. Determination of fracture energy, process zone length and brittleness number from size effect, with application to rock and concrete. Int J Fract 1990;44:111–31.
[3] Bažant ZP, Kazemi MT. Size dependence of concrete fracture energy determined by RILEM work of fracture method. Int J Fract 1991;51:121–38.
[4] Bažant ZP, Jirásek M. *R*-curve modeling of rate and size effects in quasi-brittle fracture. Int J Fract 1993;62:355–73.
[5] Ouyang CS, Mobasher B, Shah SP. An *R*-curve approach for fracture of quasi-brittle materials. Eng Fract Mech 1990;37:901–13.
[6] Jenq YS, Shah SP. Two parameter fracture model for concrete. J Eng Mech ASCE 1985;111:1227–41.
[7] Wecharatana M, Shah SP. Predictions of nonlinear fracture process zone in concrete. J Mater Civil Eng ASCE 1983;109:1231–46.
[8] Jenq YS, Shah SP. A fracture toughness criterion for concrete. Eng Fract Mech 1985;21:1055–69.
[9] Elices M, Planas J. The equivalent elastic crack. 1: load-*Y* equivalences. Int J Fract 1993;61:159–72.
[10] Planas J, Elices M, Ruiz G. The equivalent elastic crack. 2: *X*–*Y* equivalences and asymptotic analysis. Int J Fract 1993;61:231–46.
[11] Tvergaard V, Hutchinson JW. The relation between crack growth resistance and fracture process parameters in elastic-plastic solids. J Mech Phys Solids 1992;40:1377–97.
[12] Foote RML, Mai YW, Cotterell B. Crack growth resistance curves in strain-softening materials. J Mech Phys Solids 1986;34:507–93.
[13] Xu SL, Reinhardt HW. Crack extension resistance and fracture properties of quasi-brittle softening materials like concrete based on the complete process of fracture. Int J Fract 1998;92:71–99.
[14] Reinhardt HW, Xu SL. Crack extension resistance based on the cohesive force in concrete. Eng Fract Mech 1999;64:563–87.
[15] Mai YW. Cohesive zone and crack-resistance *R*-curve of cementitious materials and their fibre-reinforced composites. Eng Fract Mech 2002;69:219–34.
[16] Hu XZ, Wittmann FH. Experimental method to determine extension of fracture process zone. J Mater Civil Eng ASCE 1990;2:15–23.
[17] Kumar S, Barai SV. Determining double-K fracture parameters of concrete for compact tension and wedge splitting tests using weight function. Eng Fract Mech 2009;76:935–48.
[18] Kumar S, Barai SV. Determining the double-K fracture parameters for three-point bending notched concrete beams using weight function. Fatigue Fract Eng M 2010;33:645–60.
[19] Kumar S, Barai SV. Weight function approach for determining crack extension resistance based on the cohesive stress distribution in concrete. Eng Fract Mech 2009;76:1131–48.
[20] Kumar S, Barai SV. Influence of specimen geometry and size-effect on the K_R curve based on the cohesive stress in concrete. Int J Fract 2008;152:127–48.
[21] Kumar S, Barai SV. Influence of loading condition and size-effect on the K_R curve based on the cohesive stress in concrete. Int J Fract 2009;156:103–10.
[22] Ballarini R, Shah SP, Keer LM. Crack growth in cement-based composites. Eng Fract Mech 1984;20:433–45.
[23] Hu XZ, Wittmann FH. An analytical method to determine the bridging stress transferred with the fracture process zone: I. General theory. Cem Concr Res 1991;21:1118–28.
[24] Hu XZ, Wittmann FH. An analytical method to determine the bridging stress transferred with the fracture process zone: II. Application to mortar. Cem Concr Res 1992;22:559–70.
[25] Xu F, Wu ZM, Zheng JJ, Zhao YH, Liu K. Crack extension resistance curve of concrete considering variation of FPZ length. J Mater Civil Eng ASCE 2011;23:703–10.
[26] Chen HP. Stress singularities in anisotropic multi-material wedges and junctions. Int J Solids Struct 1998;35:1057–73.
[27] Chen HP, Guo ZY, Zhou XM. Stress singularities of contact problems with a frictional interface in anisotropic bimaterials. Fatigue Fract Eng Mater Struct 2012;35:718–31.
[28] Yang ZJ, Chen JF, Proverbs D. Finite element modelling of concrete cover separation failure in FRP plated RC beams. Construct Build Mater 2003;17:3–13.
[29] Moes N, Belytschko T. Extended finite element method for cohesive crack growth. Eng Fract Mech 2002;69:813–33.
[30] Wolf JP, Song CM. Finite-element modelling of unbounded media. Chichester: John Wiley; 1996.
[31] Ooi ET, Yang ZJ. Modelling dynamic crack propagation using the scaled boundary finite element method. Int J Numer Methods Eng 2011;88:329–49.
[32] Yang ZJ. Fully automatic modelling of mixed-mode crack propagation using scaled boundary finite element method. Eng Fract Mech 2006;73:1711–31.
[33] Xie M, Gerstle WH. Energy-based cohesive crack-propagation modeling. J Eng Mech-ASCE 1995;121:1349–58.
[34] Yang ZJ, Chen JF. Finite element modelling of multiple cohesive discrete crack propagation in reinforced concrete beams. Eng Fract Mech 2005;72:2280–97.
[35] Bittencourt TN, Ingraffea AR, Llorca J. Simulation of arbitrary cohesive crack propagation. In: Bazant ZP, editor. Fracture mechanics of concrete structures. Amsterdam: Elsevier; 1992. p. 339–50.
[36] Ooi ET, Yang ZJ. Modelling crack propagation in reinforced concrete using a hybrid finite element-scaled boundary finite element method. Eng Fract Mech 2011;78:252–73.
[37] Ooi ET, Yang ZJ. A hybrid finite element-scaled boundary finite element method for crack propagation modelling. Comput Method Appl M 2010;199:1178–92.
[38] Yang ZJ, Deeks AJ. Fully-automatic modelling of cohesive crack growth using a finite element-scaled boundary finite element coupled method. Eng Fract Mech 2007;74:2547–73.
[39] Ooi ET, Yang ZJ. Modelling multiple cohesive crack propagation using a finite element-scaled boundary finite element coupled method. Eng Anal Boundary Elem 2009;33:915–29.
[40] Xu SL, Reinhardt HW. Determination of double-determination of double-K criterion for crack propagation in quasi-brittle fracture Part I: experimental investigation of crack propagation. Int J Fract 1999;98:111–49.
[41] Xu SL, Reinhardt HW. Determination of double-K criterion for crack propagation in quasi-brittle fracture Part I: analytical evaluating and practical measuring methods for three-point bending notched beams. Int J Fract 1999;98:151–77.
[42] Petersson PE. Crack growth and development of fracture zones in plain concrete and similar materials. Division of Building Materials, Lund Institute of Technology, Report TVBM-1006, Sweden; 1981.